inorganics

MDPI

Article

Hydrogenation of Carbon Dioxide to Formate Using a Cadmium-Based Metal–Organic Framework Impregnated with Nanoparticles

Nyasha Makuve [1], James Darkwa [1], Gift Mehlana [2,*] and Banothile C. E. Makhubela [1,*]

[1] Research Centre for Synthesis and Catalysis, Department of Chemical Sciences, Auckland Park Kingsway Campus, University of Johannesburg, Auckland Park, P.O. Box 524, Johannesburg 2006, South Africa; nyashamakuve@ymail.com (N.M.); JDarkwa@bitri.co.bw (J.D.)
[2] Department of Chemical Technology, Midlands State University, Private Bag 9055 Senga Road, Gweru 263, Zimbabwe
* Correspondence: mehlanag@staff.msu.ac.zw (G.M.); bmakhubela@uj.ac.za (B.C.E.M)

Abstract: The burning of fossil fuels to meet energy demands has increased carbon dioxide (CO_2) in the atmosphere, causing global warming and associated climate change. Therefore, new materials are being developed to capture CO_2 effectively, limit its impact on the environment, and store and/or utilise it as an abundant C1 building block. In this study, we investigate a cadmium(II) metal–organic framework, $[Cd(bdc)(DMF)]_n$ (MOF1), synthesised by treating benzene-1,4-dicarboxylic acid with four equivalents of $[Cd(NO_3)_2]$. MOF1 was then used to support Pd, Ni, and Pt nanoparticles in forming MOF1/Pd MOF1/Ni and MOF1/Pt, respectively. These MOF-based materials were characterised using powder X-ray diffraction (PXRD), Fourier-transform infrared (FTIR), energy-dispersive X-ray spectroscopy (EDX), selected area electron diffraction (SAED), and high-resolution transmission electron microscopy (HR-TEM). MOF1/Pd MOF1/Ni and MOF1/Pt proved highly active in the catalytic hydrogenation of CO_2 to formate selectively; in contrast, MOF1 did not hydrogenate CO_2 to formate. The MOF1/Pd, MOF1/Ni, and MOF1/Pt catalysts produced formate selectively, with the highest TON of 1500 (TOF of 69 h^{-1}) achieved using MOF1/Pd as the catalyst at 170 °C within 2 h. A formate yield of 98% was obtained, which demonstrates that the combination of nanoparticles and MOFs greatly enhances the catalytic activity of the active sites.

Keywords: CO_2 catalytic hydrogenation; heterogeneous catalysis; MOF; formate

check for updates

Citation: Makuve, N.; Darkwa, J.; Mehlana, G.; Makhubela, B.C.E. Hydrogenation of Carbon Dioxide to Formate Using a Cadmium-Based Metal–Organic Framework Impregnated with Nanoparticles. *Inorganics* **2022**, *10*, 30. https://doi.org/10.3390/inorganics10030030

Academic Editor: Lars Öhrström

Received: 26 October 2021
Accepted: 26 January 2022
Published: 25 February 2022

Publisher's Note: MDPI stays neutral with regard to jurisdictional claims in published maps and institutional affiliations.

Copyright: © 2022 by the authors. Licensee MDPI, Basel, Switzerland. This article is an open access article distributed under the terms and conditions of the Creative Commons Attribution (CC BY) license (https://creativecommons.org/licenses/by/4.0/).

1. Introduction

Hydrogenation of CO_2 has been more intensively investigated recently due to fundamental and practical significance in the context of catalysis, surface science, biology, nanoscience and nanotechnology, and environmental science [1]. Catalysis provides tools for efficiently and selectively making and breaking chemical bonds crucial for converting given chemicals into more valuable products. Both homogeneous and heterogeneous catalysts have been used to hydrogenate CO_2. Homogeneous hydrogenation of CO_2 to formic acid has been achieved in aqueous solutions using mainly rhodium and ruthenium catalyst [2].

Formic acid is a starting material for producing, for example, formate esters, which allows access to a range of useful organic derivatives such as aldehydes, ketones, carboxylic acids, and amides. Such commercially C1 (CO_2) based products and intermediates include urea, salicylic acid, and polyols. In 2012, the global production of formic acid was 620 kt, and this was predicted to surpass 760 kt in 2019. It has recently been shown in a life-cycle assessment of C1-based chemicals that the production of formic acid achieves the highest environmental impact reductions. Moreover, "CO_2-based production of formic acid can reduce environmental impacts, compared to the fossil-based process, even if hydrogen is supplied by fossil-based steam-methane reforming".

While homogeneous catalysts show satisfactory activity and selectivity, recovery and regeneration are problematic [3,4]. Alternatively, heterogeneous catalysts offer better stability, separation, handling, and reuse, as well as more straightforward reactor design, which reflects lower costs for large-scale productions [5]. However, the vast majority of these reactions are far from ideal (limited selectivity, stoichiometric conversions), and therefore, other breakthrough technologies that proceed under mild conditions are required.

The upsurge of interest in the synthesis and design of metal–organic frameworks (MOFs) has been due to their high degree of microporous architecture. They have gained remarkable functions in catalysis, gas storage, and separation [6,7]. Of late, there has been much interest in using the MOF pores for nanoparticle (NPs) encapsulation. The combination of MOFs and NPs is a promising hybrid technique for catalysis due to their high surface area, pore size, and enormous functional properties [8]. MOFs are synthesised by various techniques such as solvothermal, hydrothermal, microwave, electrochemical, mechanochemical, and sonochemical techniques [9–11]. The solvothermal technique is the most commonly used due to its liquid-phase reaction mixture and provides a wide range of reaction conditions such as temperature, reaction time, and solvents. Incorporating NPs in MOFs can be accomplished by solid grinding, solvent-free gas-phase loading, microwave irradiation, solution impregnation, and incipient wetness impregnation [12–15]. None of these methods allows specific control over the NPs loading within the MOF crystals.

Nanoparticles have been encapsulated in water-stable MOFs to hydrogenate CO_2 to methanol at 170 °C. In this regard, Zr-based MOFs have been used as support MOFs due to their high chemical stability and large surface area. Olsbye et al. used UiO67 MOFs to support Pt nanoparticles. Their study provides evidence that methanol was formed at the interface of Pt nanoparticles and the linker deficient secondary building unit nodes resting on the Pt nanoparticle surface [16,17]. A related study noted that the Cu nanocrystals' activity and selectivity can be promoted by encapsulating them in a Zr-based MOF UiO-66. The performance of this catalyst construct exceeds the benchmark $Cu/ZnO/Al_2O_3$ catalyst and gives a steady eightfold enhanced yield and 100% selectivity for methanol [8].

As part of our ongoing research on CO_2 utilisation [18,19], we have taken advantage of the chemical stability offered by the cadmium MOFs [20] under different solvent conditions and the high activity offered by nanoparticles towards CO_2 hydrogenation. Nanoparticles of Ni, Pd, and Pt were encapsulated in the activated MOF1. Hydrogenation studies revealed a significant increase in the yield of formate obtained from MOF nanoparticles composite compared to unsupported nanoparticles. The MOF encapsulated with Pd nanoparticles could be recycled five times without significant loss in the catalytic activity.

2. Experimental

2.1. Materials and Methods

All air- and moisture-sensitive compounds were manipulated using standard Schlenk and vacuum line techniques under an argon atmosphere. Argon HP/zero-grade, carbon dioxide HP/zero-grade gas, and hydrogen gas HP/zero-grade (>99%) cylinders were purchased from Afrox Gases. Benzene-1,4-dicarboxylic acid (Aldrich, >98%), triethylamine (Aldrich, >99%), $NiCl_2$ (Aldrich, 98%), $Cd(NO_3)_2$. $4H_2O$ (Aldrich, >99%), *N*,*N*-dimethylformamide anhydrous (DMF, Aldrich, >99.8%), sodium borohydride (Aldrich, >99%), acetonitrile anhydrous (CH_3CN) (Aldrich, >99%) and 1,8-diazabicyclo [5.4.0] undec-7-ene (DBU) (Aldrich, 98%) were purchased from Sigma-Aldrich, South Africa. Potassium hydroxide, absolute ethanol, acetonitrile, toluene, tetrahydrofuran (THF), and dimethyl sulfoxide (DMSO) were purchased from Rochelle Chemicals South Africa. $PdCl_2$ and $K_2[PtCl_4]$ were purchased from Heraeus Metals, South Africa. ^1H and ^{13}C NMR spectra were recorded on a Bruker Ultrashield 400 MHz (^1H: 400 MHz; ^{13}C:100 MHz) spectrometer. Spectrometer values were reported relative to the internal standard tetramethylsilane (δ 0:00). All chemical shifts were reported in ppm. ^1H and $^{13}C\{^1H\}$ NMR chemical shifts for the hydrogenation products were determined relative to the internal standard mesitylene. FTIR spectra were recorded using a PerkinElmer FTIR Spectrum BX Spectrometer. Ther-

mogravimetric experiments were carried out using a TA Discovery Instrument TA-Q50. High-resolution transmission electron microscopy (HR-TEM) images were obtained on a JOEL JEM-1200F electron microscope with an acceleration voltage of 200 kV. The average particle sizes were obtained by analysing HR-TEM images by ImageJ software. Powder diffraction patterns (PXRD) were measured on a Bruker D8 Advance X-ray diffractometer operating in a DaVinci geometry equipped with a Lynxeye detector using a CuKα radiation (λ = 1.5406 Å). The XSEED program was used to obtain calculated PXRD patterns from the corresponding single crystal data.

2.2. Synthesis and Characterisation of Cd(bdc)(DMF)$_n$(MOF1)

Benzene-1,4-dicarboxylic acid (bdc) (40.00 mg, 0.241 mmol) and $Cd(NO_3)_2{\cdot}4H_2O$ (300.00 mg, 0.975 mmol) were mixed in DMF (5 mL), and the solution was stirred for 20 min at 50 °C before heating in an oven for 24 h at 90 °C. Colourless, rod-like crystals were obtained.

2.3. Preparation of Pd, Pt, and Ni Nanoparticles

To prepare nanoparticles of Pd, 6.68×10^{-2} mmol of PdCl2 and 67.6×10^{-2} mmol of polyvinylpyrrolidone (PVP) (Mw 55000) were dissolved and stirred in a three-neck, round-bottom flask in 20 mL of tri-ethylene glycol (TEG) at 220 °C for 3 h under N_2 atmosphere. A similar method was also used to prepare Pt and Ni nanoparticles.

2.4. Preparation of MOF1/Pd, MOF1/Ni, and MOF1/Pt

MOF1 was activated heating in an oven at 150 °C for 24 h [21,22]. The encapsulation of Pd^0, Ni^0, and Pt^0 nanoparticles into the activated MOF1 to produce MOF1/Pd, MOF1/Ni, and MOF1/Pt, respectively, was carried out by soaking the respective nanoparticles (Pd^0, Ni^0, and Pt^0) into activated MOF1 according to the solution impregnation method reported in the literature [23]. To prepare MOF1/Pd, MOF1/Pt, and MOF1/Ni, 10 mL colloidal solution of the respective nanoparticles were impregnated on 200 mg of activated MOF1 in 10 mL of acetone and mixed for 2 h at 50 °C by using a magnetic stirrer. After the solids settled, the liquid phase was decanted to remove TEG from the solvent and surface of the composite materials. This step was repeated four times. Finally, the obtained powder was dried in an oven at 100 °C for 2 h. The exact metal loading was determined by ICP–OES.

2.5. General Procedure for CO_2 Hydrogenation Experiments

In a typical experiment, the precatalysts MOF1, MOF1/Pd, MOF1/Ni, and MOF1/Pt (3 µmol), KOH (5.00 mmol), and THF (8 mL) were mixed in separate 50 mL stainless steel autoclaves. The reactor vessels were flushed with three cycles of nitrogen gas, followed by the addition of CO_2 gas and H_2 gas (1:3, CO_2:H_2 bar) to make a total pressure of 30 bar. Subsequently, the reactor vessels were heated in a preheated EYELA reactor block at 170 °C and a stirring speed of 1000 rpm for 24 h. After reaction completion, the reactor was cooled to room temperature, followed by carefully venting. The reaction mixture was analysed by ^{1}H NMR and $^{13}C\{^1H\}$ NMR spectroscopy, using CH_3CN as an internal standard.

3. Results and Discussion

3.1. Structural Description

MOF1 was previously reported by Burrows et al. [20]. The asymmetric unit of MOF1 consists of one cadmium centre coordinated to two anions of bdc ligand and one DMF molecule. The Cd (II) is coordinated to the carboxylate of the bdc in a bidentate chelating mode. The cadmium metal centre is a six-coordinate bonded to one DMF molecule and two different sets of carboxylates from two different bdc ligands, whilst the remaining portion of the bdc anion is generated by inversion symmetry. The bridging oxygen (O(2A)/O(2B)) bond to the cadmium metal by donating electrons in the sp^3 d^2 hybridised orbitals. The secondary building unit (SBU) of MOF1 growing along the b-axis is made up of $Cd_2C_2O_4$. MOF1 consists of rhomboidal pores occupied with the coordinated DMF

molecule, thus reducing the void space. Figure 1 shows the structural features of MOF1, viewed along the a-axis. PXRD studies shown in Figure 2 demonstrate successful synthesis of MOF1, as revealed by the excellent agreement between the experimental and calculated patterns. This match also confirms the phase purity of the bulk material. As previously reported, the structural integrity of the MOF is maintained upon removal of the DMF molecules.

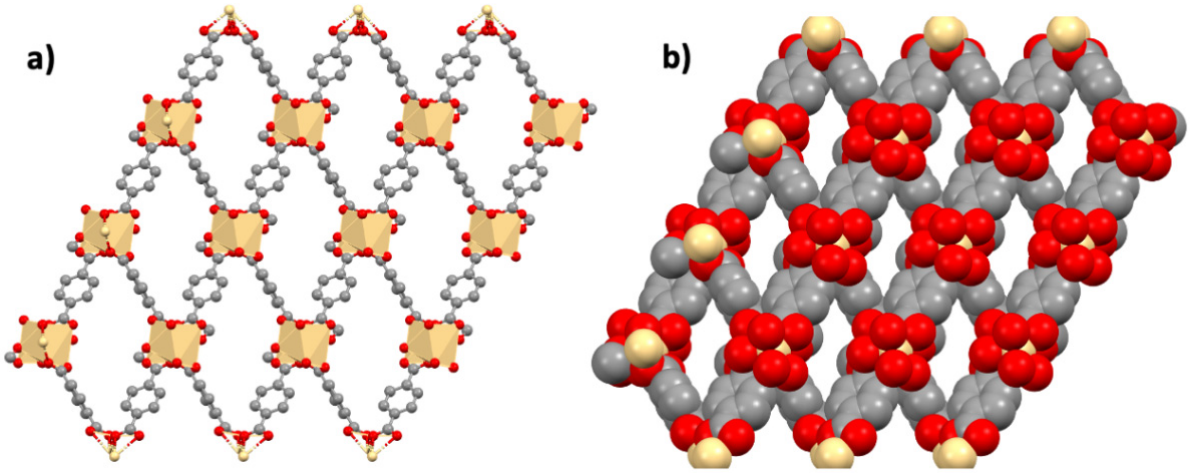

Figure 1. MOF1 viewed along the a-axis, coordinated DMF molecules have been omitted: (**a**) polyhedral representation; (**b**) MOF 1 drawn using the van der Waals radii. The guest molecules which occupy the channels are omitted.

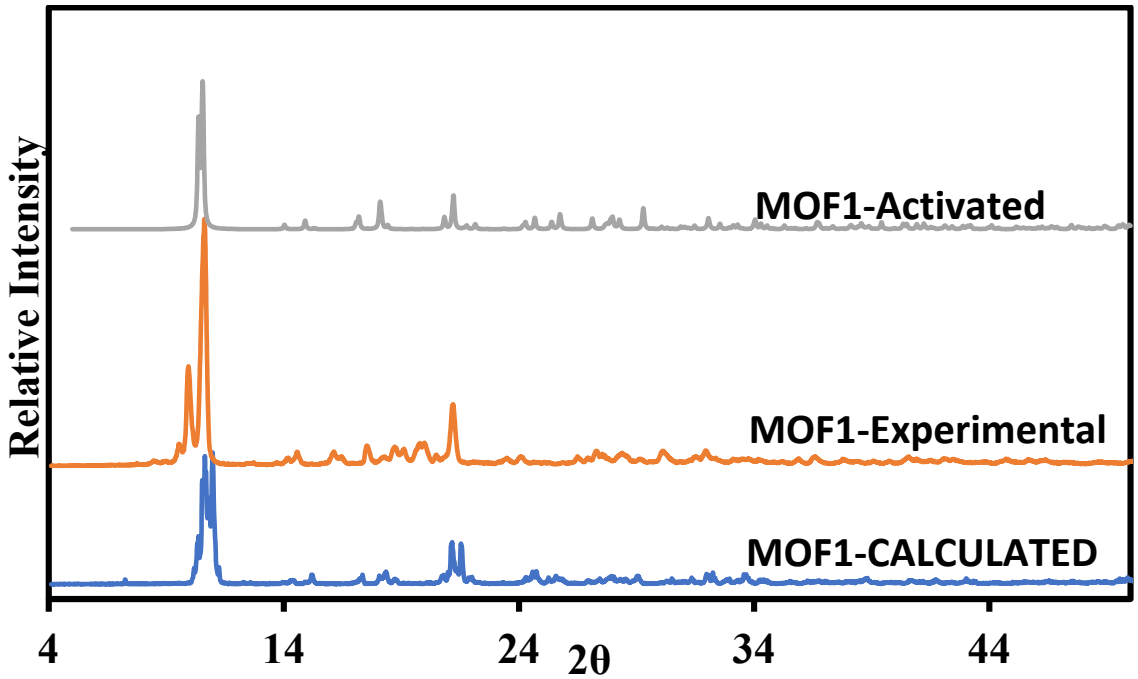

Figure 2. PXRD pattern for MOF1 overlaid with calculated PXRD pattern for MOF1.

3.2. PXRD Analysis for MOF1/Pd, MOF1/Ni, and MOF1/Pt

The structural integrity of the activated MOF1 upon incorporating nanoparticles in the pores was probed by PXRD studies. Figure 3 shows the PXRD patterns of MOF1/Pd, MOF1/Ni, MOF1/Pt, and MOF1, which are stacked for easy comparison. As depicted in Figure 3, the PXRD patterns for MOF1/Pd, MOF1/Ni, and MOF1/Pt concur with MOF1 PXRD, suggesting that the integrity of the MOF is preserved upon encapsulation of the

nanoparticles. PXRD patterns for MOF1/Pd, MOF1/Ni, and MOF1/Pt show intense peaks around 38 and 43, two thetas, indicating the formation of nanoparticles with sizes exceeding 4–5 nm.

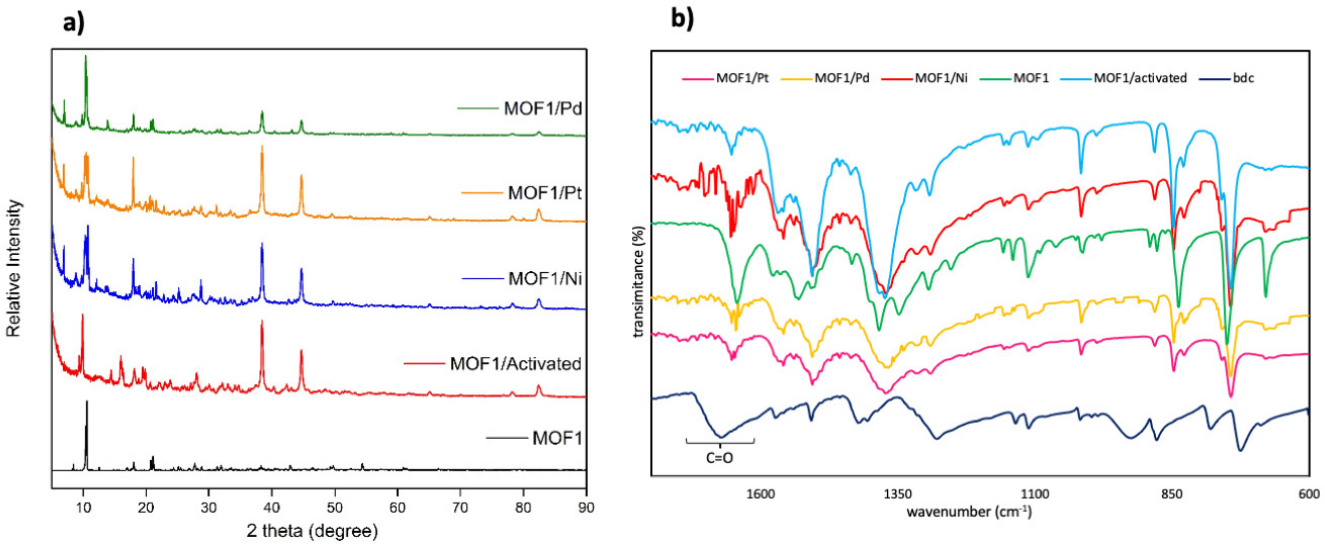

Figure 3. (**a**) PXRD pattern for MOF1; the line labelled as MOF1 is related to the raw MOF1, while that labelled as MOF1/activated is related to MOF1 after solvent soaking and heating; (**b**) FTIR spectra of MOF1 and its composites.

FTIR studies (Figure 3b) were used to identify the characteristic carboxylate moiety (C=O) and probe change in binding mode upon metalation during MOF synthesis. The C=O stretching observed in the linker (bdc) at 1666 cm^{-1} shifted to a lower absorption band of 1652 cm^{-1} in MOF1. This is a clear indication of the metalation process of bdc. The FTIR spectra of MOF1, MOF1/Pt, MOF1/Pd, and MOF1/Ni display similar characteristic bands that further support the XRD studies' data, indicating that the carboxylate moiety's binding mode is not affected in the MOF composites.

3.3. Thermal Analysis

TGA was used to analyse the thermal stability of MOF1 and its nanoparticle encapsulated derivatives. Thermal analysis of MOF1 by TGA (Figure 4) shows a 22.6% weight loss between 158 °C and 366 °C. Most of this calculated weight loss, 20.9%, represents coordinated DMF modelled on the crystal structure of MOF1, while the remaining 2% is due to absorbed moisture. Decomposition of the framework is observed above 415 °C. The activated MOF1 TGA thermogram is featureless between 200 °C and 400 °C, indicating thermal stability MOF1/Pd, MOF1/Pt, and MOF1/Ni exhibited similar thermal profiles to MOF1, as illustrated in Figure 4.

3.4. High-Resolution Electron (HR-TEM) Spectroscopy, ICP–OES, and EDX Analysis

High-resolution transmission electron microscopy (HR-TEM) micrographs of MOF1/Pd show spherical nanoparticles distribution with an average particle size diameter of 3.4 nm and standard deviation of ±0.6 nm (Figure 5).

The SAED pattern for MOF1/Pd (Figure 5d) further confirms its crystalline nature. Similar SAED patterns were observed for MOF1/Pt and MOF1/Ni (Figure S1). Both MOF1/Pt and MOF1/Ni had spherical nanoparticles with an average particle size distribution of 3.2 ± 0.5 nm and 3.1 ± 0.4 nm, respectively. Hou and Lei reported similar results after synthesising Ni and Pt nanoparticles with an average of 3 nm diameter [24,25]. MOF1/Pd, MOF1/Ni and MOF1/Pt contain Pd 2.44% m/m, Pt 2.75% m/m, and Ni 0.86% m/m, respectively. These composites' detailed quantitative chemical analysis was carried out using EDX (Figure S2). All compounds contained C, O, and Cd as the main compo-

nents with Pd, Ni, and Pt observed in MOF1/Pd, MOF1/Ni, and MOF1/Pt, respectively. Scanning electron microscopy (SEM) and energy-dispersive spectroscopy (EDS) were used for elemental mapping analysis. The results shown in Figure S3 reveal that Pt, Pd, and Ni nanoparticles are fairly distributed within the activated MOF1 matrix.

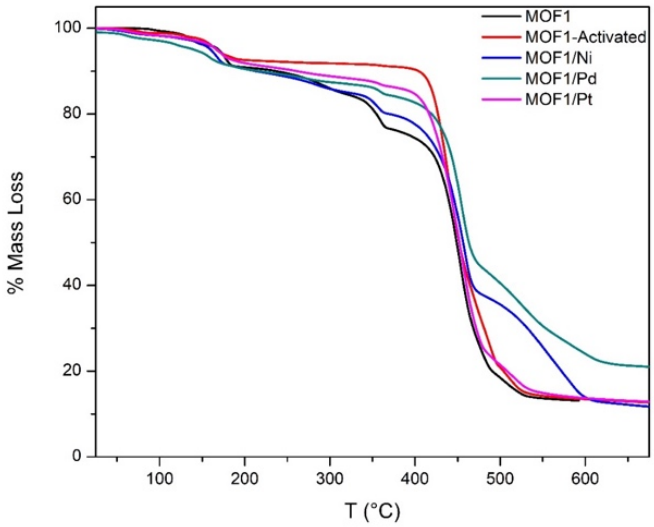

Figure 4. Thermal profiles of MOF1 and its derivatives.

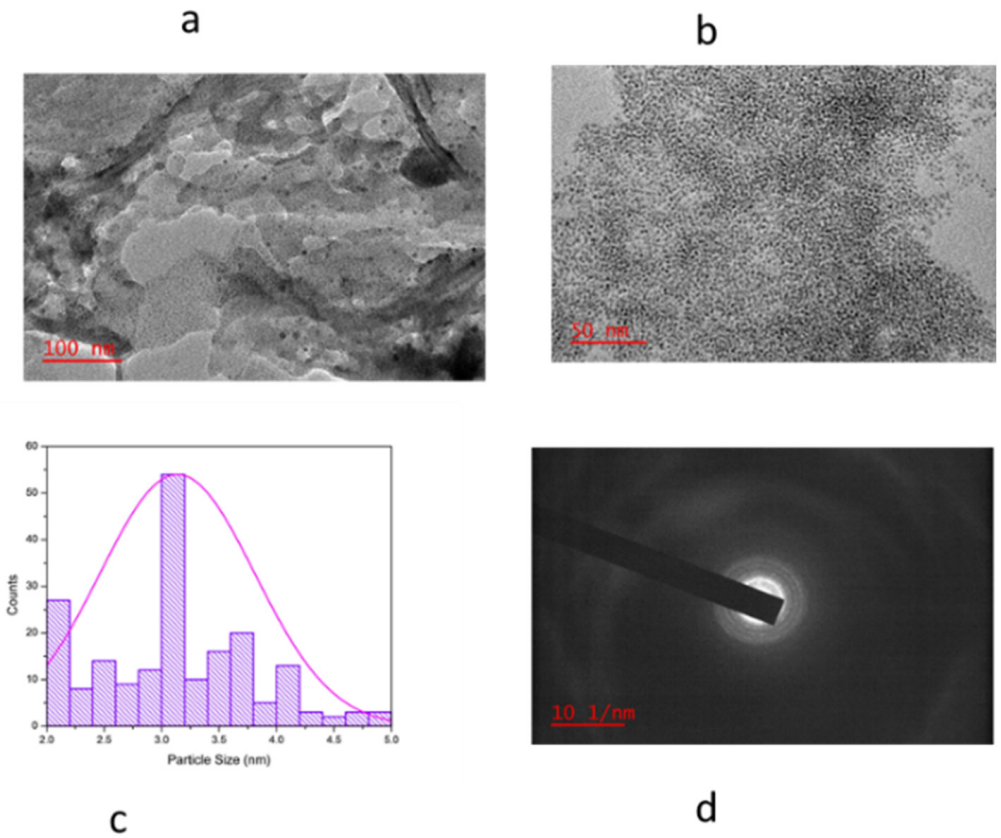

Figure 5. HR-TEM images for MOF1/Pd at (**a**) 100 nm, (**b**) 50 nm scale, (**c**) histogram of the particle size distribution for MOF1/Pd and SAED, and (**d**) SAED pattern.

3.5. Chemical Stability Studies

Having confirmed the synthesis of MOF1 using various analytical techniques, it was essential to check its chemical stability in the presence of solvents and bases, which are

typically used in the hydrogenation of CO_2 to formate. MOF1 was activated by heating the as-made crystals in an oven at 150 °C for 24 h before being subjected to different solvents and bases. Polycrystalline powders of the activated MOF1 were soaked in ethanol (8 mL), water (8 mL), THF/water (7 mL/1 mL), THF/triethylamine (8 mL/5 mmol), THF/DBU (8 mL/5 mmol), and THF/KOH (8 mL/5 mmol) for 24 h, and the PXRD results are shown in Figure 6.

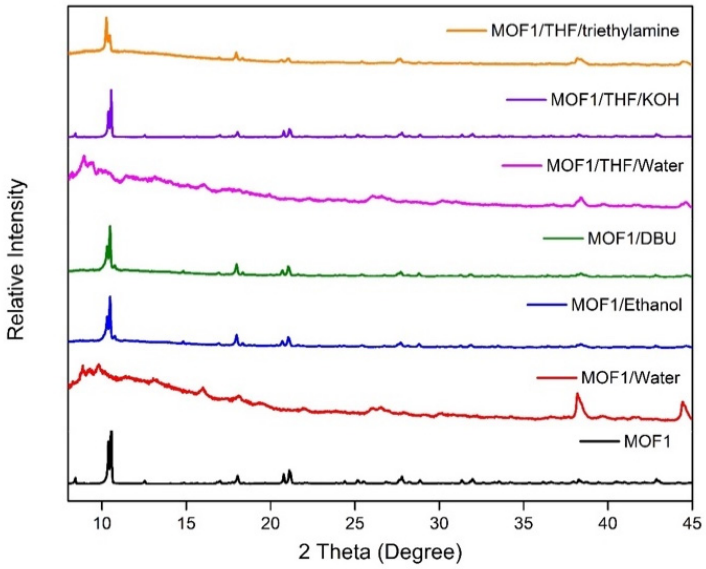

Figure 6. PXRD patterns of activated MOF1 soaked in different solvents and bases used for CO_2 hydrogenation to formate.

PXRD studies revealed that the activated MOF1 was highly unstable in water and a water/THF solvent mixture, as seen from the diffraction pattern change. The structural integrity of the MOF is maintained in ethanol, DBU, THF/KOH mixture, and THF/triethylamine mixture. These results show that the hydrogenation of CO_2 can be performed using these solvents and bases, which do not compromise the framework of the MOF.

Catalysis Studies

The multifunctional properties of MOFs are derived from the organic backbone and the metal clusters; therefore, during catalysis, it is essential to understand the origin of the active species [26,27]. Considering this point, activated MOF1 without nanoparticles was tested for the hydrogenation of CO_2 to formate according to Scheme 1.

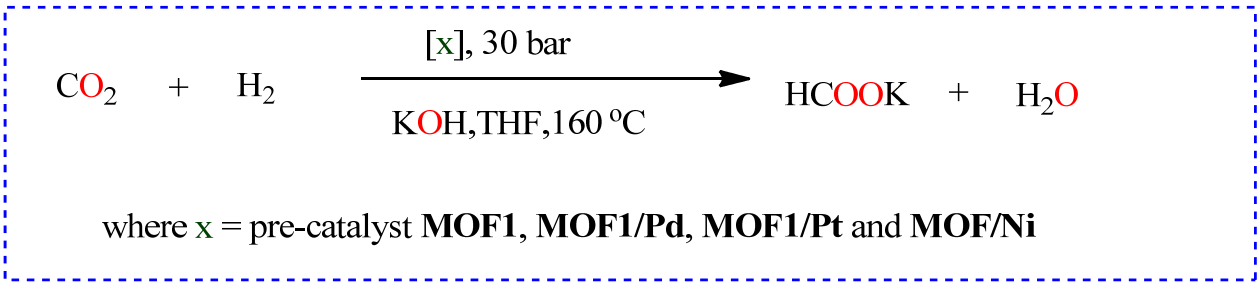

Scheme 1. CO_2 hydrogenation to formate with MOF1, MOF1@Pd, MOF1@/Pt, and MOF1@Ni in the presence of KOH base.

The hydrogenation of CO_2 to formate proceeded with base variations in the presence of MOF1 in THF solvent at 160 °C, and the results are shown in Table 1. As evident from

the results of CO_2 hydrogenation in the presence of organic bases Et_3N and DBU (Table 1; Entries 1 and 2), no conversion of CO_2 to formate was observed; however, the solution became a homogeneous solution after the reaction instead of a heterogeneous mixture as it was at the start of the reaction. This phenomenon shows that MOF1 was chemically unstable under these reaction conditions. In comparison, in the hydrogenation of CO_2 with MOF1 in the presence of KOH base in THF (Entry 3), no conversion of CO_2 to formate was observed; however, the system maintained its heterogeneity. The inorganic base KOH was found to be the optimum base for the hydrogenation of CO_2 under our reaction conditions. Activated MOF1 is not catalytically active in CO_2 hydrogenation since no formate was produced in a reaction with MOF1 in catalytic amounts.

Table 1. Catalytic hydrogenation studies of CO_2 with activated MOF1 in the absence of nanoparticles.

Entry	Cat.	Cat. (μmol)	Temp/(°C)	Base	Ratio CO_2/H_2	HCOO (mmol)	TON	Yield (%)	TOF (h^{-1})
1 [a]	MOF1	3.00	160	Et_3N	1:3	-	-	-	-
2 [a]	MOF1	3.00	160	DBU	1:3	-	-	-	-
3	MOF1	3.00	160	KOH	1:3	-	-	-	-

Conditions: KOH (5.00 mmol), total pressure 30 bar, THF (8 mL), and 24 h. Cat. = precatalyst loading (μmol). Products were determined by ^1H NMR and $^{13}C\{^1H\}$ NMR spectroscopy in the presence of CH_3CN (5 μL) as an internal standard. [a] forms a homogeneous solution after catalysis.

The hydrogenation of CO_2 with MOF1/Pd, MOF1/Ni, and MOF1/Pt (Table 2; Entry 1–3) showed formate production. MOF1/Ni produced 0.11 mmol of formate, which was the lowest, and MOF1/Pd had the highest, producing 3.1 mmol of formate, with a yield of 62% and a TON value of 1033. The hydrogenation of CO_2 in the presence of unsupported nanoparticles of Pd, Pt, and Ni (Entry 4–6) produced formate, though it was less than in the presence of nanoparticles supported on MOF1. With these findings, we can deduce that the hydrogenation of CO_2 to formate can only occur in the presence of nanoparticles that are the active species for CO_2 hydrogenation. Supporting nanoparticles on MOF1 increased the activity of CO_2 hydrogenation, suggesting stabilisation of the nanoparticles by MOF1, thereby minimising nanoparticle agglomeration.

Table 2. Hydrogenation of CO_2 with MOF1/Pd, MOF1/Pt, and MOF1/Ni.

Entry	Cat.	Base	Ratio CO_2:H_2	HCOO (mmol)	TON	Yield (%)	TOF (h^{-1})
1	MOF1/Pd	KOH	1:3	3.1	1033	62	43
2	MOF1/Pt	KOH	1:3	1.9	633	44	26.4
3	MOF/Ni	KOH	1:3	0.11	37	2.2	1.5
4	Pd/NPs	KOH	1:3	2.3	782	46	33
5	Pt/NPs	KOH	1:3	1.3	437	26	19
6	Ni/NPs	KOH	1:3	0.05	17	1	0.7
7	MOF1/Pd	No base	1:3	-	-	-	-
8 [b]	MOF1/Pd	KOH	1:3	-	-	-	-
9 [c]	MOF/Pd	KOH	1:3	-	-	-	-
10 [d]	MOF1/Pd	KOH	1:3	1.9	633	38	53
11 [e]	MOF1/Pd	KOH	1:3	0.41	137	8.2	69
12	MOF1/Pd	KOH	1:2	2.1	700	42	29

Having identified the best performing precatalyst MOF1/Pd, CO_2 hydrogenation was carried out without a base (Entry 7), resulting in no formate production. This inactivity shows that the reaction is base assisted. In the absence of a solvent (Entry 8) and changing the solvent to ethanol (Entry 9), no conversion of CO_2 was observed. THF was maintained as the optimum solvent for the hydrogenation of CO_2 to formate with MOF1/Pd. A shorter reaction time of 12 h (Entry 10) resulted in decreased formate yield to 38%. The decrease indicates that the yield of formate produced increases with reaction time. A

further reduction in reaction time to 2 h (Entry 11) saw the highest TOF of 69 h^{-1} recorded. Varying the partial pressure ratio of CO_2/H_2 to 1:2 (Entry 12) decreased the formate yield to 42% and a TON value of 700, compared with a ratio of 1:3, which had a yield of 62% TON value of 1033. This decrease can be attributed to the H_2 dependence of the reaction since H_2 is used to generate the catalytically active hydride species. Figures S4 and S5 show a typical ^1H NMR and $^{13}C\{^1H\}$ spectra with formate observed at 8.26 ppm and 170.90 ppm, respectively, after CO_2 hydrogenation in the presence of MOF1/Pd, in THF and KOH base.

Conditions: KOH (5.00 mmol), total pressure 30 bar, THF (8 mL), and 24 h. Cat. = precatalyst loading (µmol). Products were determined by ^1H NMR and $^{13}C\{^1H\}$ NMR spectroscopy in the presence of CH_3CN (5 µL) as an internal standard. [a] forms a homogeneous solution after catalysis, [c] ethanol, [b] no solvent, [d] reaction time = 12 h, and [e] reaction time = 2 h. Average error estimate: MOF1 = ± 0.21, MOF1/Pd = ± 0.25, MOF1/Ni = ± 0.19, MOF1/Pt= ± 0.20. TON = mmol of formate/mmol of precatalyst; TOF = TON/reaction time. Yield (%) was calculated basing on the conversion of 5 mmol added base.

3.6. Temperature and Catalyst Load Effect on Precatalysts MOF1/Pd Activity

The effect of temperature on forming formate was evaluated using MOF1/Pd, which was the best performing precatalyst under standard conditions (catalyst (3.00 µmol), KOH (5.00 mmol), total pressure = 30 bar, and $P(CO_2)/P(H_2)$ pressure ratio = 1:3; Figure 7. According to Figure 7a, the conversion of CO_2 to formate in the presence of MOF1/Pd gradually increases with an increase in temperature. The highest formate yield (90%) was obtained at 170 °C. The temperature was not raised above 170 °C due to the type of EYELA reactor systems used for these reactions. MOF1/Pd is a highly active precatalyst at moderate reaction conditions, compared with the literature reported temperatures above 250 °C for heterogeneous catalysts for CO_2 hydrogenation [28]. For further optimisation studies, 170 °C was taken as the optimum temperature.

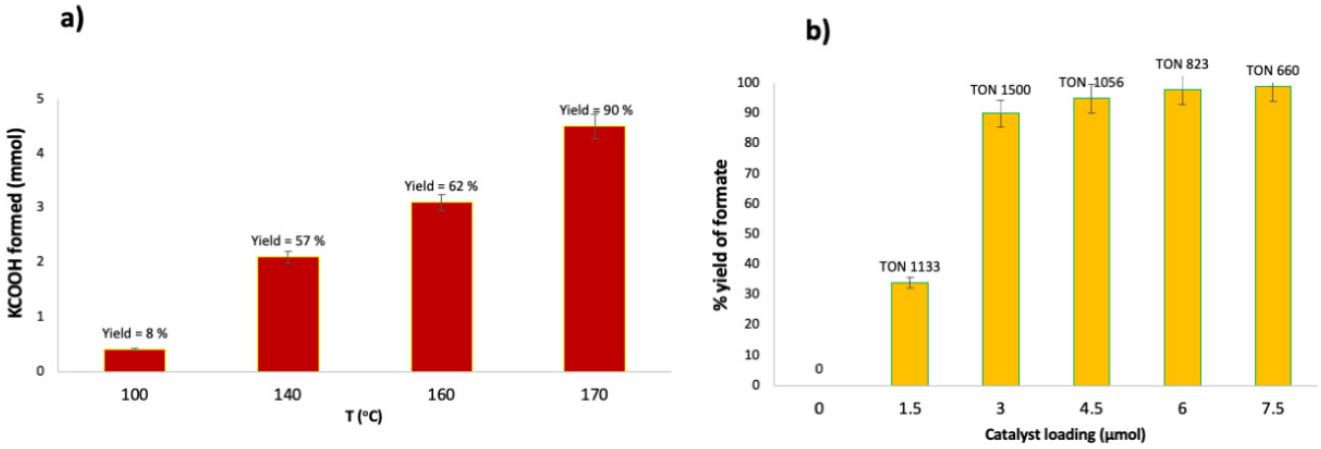

Figure 7. (**a**) Effect of temperature on CO_2 hydrogenation with precatalyst MOF1/Pd. Conditions: precatalysts (3.00 µmol), KOH (5.00 mmol), total pressure 30 bar (CO_2:H_2 (1:3), 100–180 °C, 24 h, and THF (8 mL). Products were determined by ^1H NMR and $^{13}C\{^1H\}$ NMR spectroscopy in the presence of CH_3CN (5 µL) as an internal standard. TON = mmol of formate/mmol of precatalyst; TOF = TON/reaction time. Yield (%) was calculated based on the conversion of 5 mmol added base; (**b**) effect of catalyst loading on CO_2 hydrogenation. Conditions: precatalysts (0–7.5 µmol), KOH (5.00 mmol), CO_2:H_2 (1:3 (total pressure 30 bar), 170 °C, 24 h, and THF (8 mL). Products were determined by ^1H NMR and $^{13}C\{^1H\}$ NMR spectroscopy in the presence of CH_3CN (5 µL) as an internal standard. TON = mmol of formate/mmol of precatalyst; TOF = TON/reaction time. Yield (%) was calculated based on the 5 mmol added base conversion.

The effect of catalyst loading was performed on MOF1/Pd, and the results are shown in Figure 7b. Without a precatalyst, no conversion of CO_2 was observed, indicating the

importance of a catalyst to convert CO_2 to formate. Increasing the catalyst loading from 1.00 µmol to 6.00 µmol increased the catalyst activity, thus increasing formate production. An increase in catalyst loading beyond 6.00 µmol had no significant effect on the formate produced.

3.7. CO_2 Hydrogenation under Optimised Conditions

The hydrogenation of CO_2 to formate in the presence of MOF1/Pd, MOF1/Pt, and MOF1/Ni catalyst precursors was performed under optimised conditions, and the results are shown in Figure 8. Hydrogenation of CO_2 with MOF1/Pt and MOF1/Ni had a formate yield of 64% and 11%, respectively. The best performing precatalyst was MOF1/Pd, with a formate yield of 98% achieved in the presence of KOH base and THF at 170 °C after 24 h.

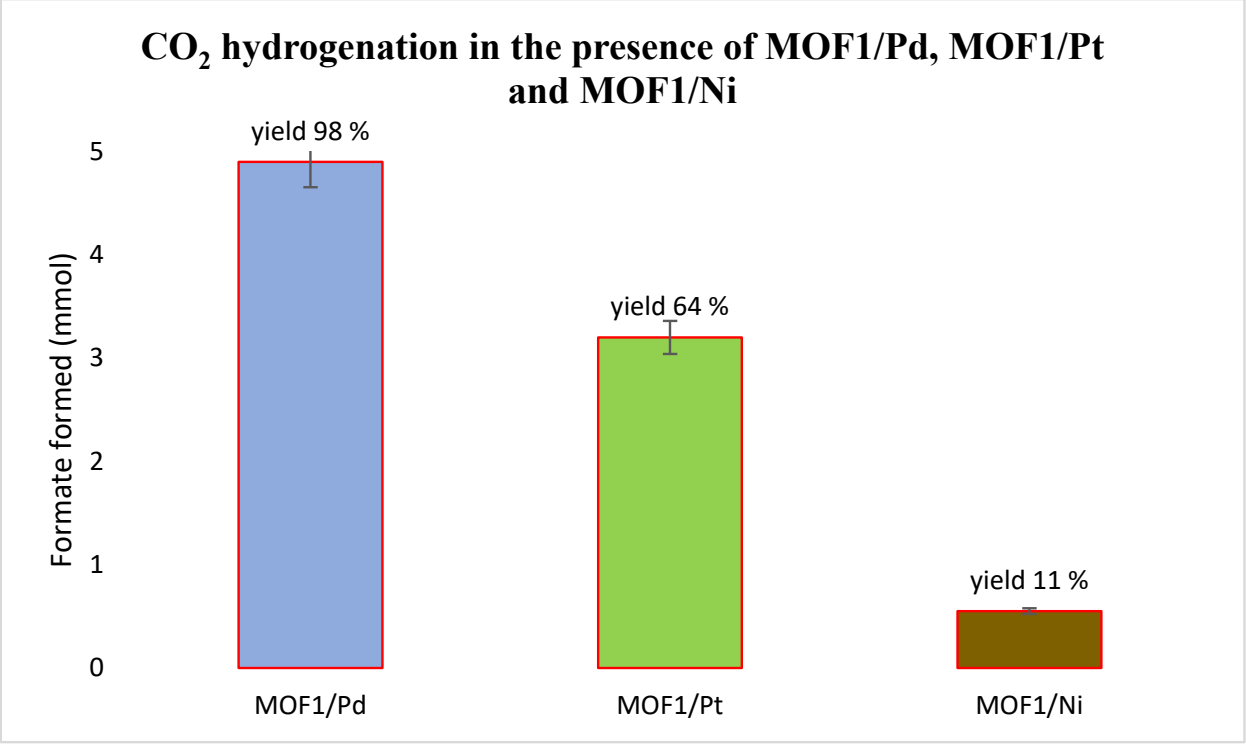

Figure 8. CO_2 hydrogenation with precatalysts MOF1/Pd, MOF1/Pt and MOF1/Ni. Conditions: precatalysts (6.00 µmol), KOH (5.00 mmol), CO_2:H_2 (1:3 (total pressure 30 bar), 170 °C, 24 h, and THF (8 mL). Products were determined by ^{1}H NMR and $^{13}C\{^1H\}$ NMR spectroscopy in the presence of CH_3CN (5 µL) as an internal standard. TON = mmol of formate/mmol of precatalyst; TOF = TON/reaction time. Yield (%) was calculated based on the 5 mmol added base conversion.

3.8. Reusability and Leaching of MOF1/Pd, MOF1/Ni, and MOF1/Pt during CO_2 Hydrogenation

The reusability of precatalysts MOF1/Pd, MOF1/Ni, and MOF1/Pt was investigated in the hydrogenation of CO_2 to formate, and the first run was performed in 5 mmol KOH and THF under at 170 °C and a total pressure of 30 bar for 24 h. MOF1/Pd, MOF1/Ni, and MOF1/Pt had a formate yield of 98%, 11%, and 64%, respectively, recorded as the first run. After the first run, the respective precatalysts were separated by filtration, washed with THF, and dried, followed by PXRD analysis. The PXRD studies after the first run (Figure 9) show the minimum change in the structural integrity of all the three precatalysts compared with MOF1. ICP–OES analysis of the aqueous solution of MOF1/Pd, MOF1/Ni, and MOF1/Pt after CO_2 hydrogenation showed negligible metal leach (0.0001%) for the respective precatalysts.

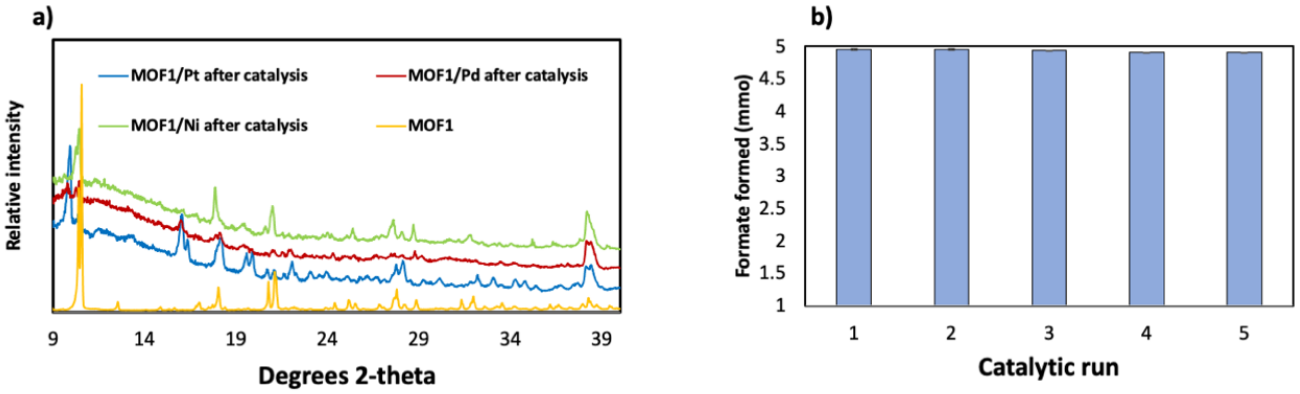

Figure 9. (**a**) PXRD studies for MOF1/Pd, MOF1/Pt, and MOF1/Ni after the first catalytic run; (**b**) CO_2 hydrogenation with precatalyst MOF1/Pd. Conditions: precatalysts (6.00 μmol), KOH (5.00 mmol), CO_2:H_2 (1:3 (total pressure 30 bar), 170 °C, 24 h, and THF (8 mL). Products were determined by ^{1}H NMR and $^{13}C\{^1H\}$ NMR spectroscopy in the presence of CH_3CN (5 μL) as an internal standard. TON = mmol of formate/mmol of precatalyst; TOF = TON/reaction time. Yield (%) was calculated based on the conversion of 5 mmol added.

The best performing precatalyst MOF1/Pd was used to demonstrate the recyclability of the prepared precatalysts. The initial hydrogenation was performed in the presence of MOF1/Pd (6. 00 μmol), KOH base (5 mmol), at a temperature of 170 °C, at a total pressure of 30 bar, and in the presence of THF. After the initial CO_2 hydrogenation run, MOF1/Pd was separated by filtration, washed thoroughly with THF, and dried. The washed and dried MOF1/Pd was then used for CO_2 hydrogenation with fresh substrates. MOF1/Pd could be used over 5 runs without significantly decreasing the yield of formate produced (Figure 9b).

4. Conclusions

Cd(II) metal–organic framework (MOF1) was successfully synthesised and fully characterised. MOF1 was successfully used to support Pd, Ni, and Pt nanoparticles to form MOF1/Pd, MOF1/Ni, and MOF1/Pt, respectively, which were fully characterised by PXRD FTIR EDX, SAED, and HR-TEM analytical techniques. MOF1, MOF1/Pd, MOF1/Ni, and MOF1/Pt were evaluated as precatalysts in the hydrogenation of CO_2 to formate. MOF1 could not hydrogenate CO_2 to formate, whilst MOF1/Pd, MOF1/Ni, and MOF1/Pt produced formate. The highest TON of 1500 was achieved with MOF1/Pd at 170 °C, and TOF of 69 h^{-1} was achieved within 2 h. A formate yield of 98% was obtained with MOF1/Pd in the presence of THF and KOH. Encapsulating nanoparticles on a MOF1 increased their catalytic activity towards forming formate with 4.9 mmol of formate produced, compared with 2.3 mmol produced with unsupported nanoparticles. MOF1 support was chemically stable under our hydrogenation conditions, which was revealed by PXRD patterns after one catalytic run.

Supplementary Materials: The following supporting information can be downloaded at: https://www.mdpi.com/article/10.3390/inorganics10030030/s1, Figure S1: HR-TEM images for MOF1@Pt and MOF1@Ni at (a and e) 100 nm, (b and f) 50 nm, (c and g) 20 nm scale and (d and h) histogram of particle size distribution; Figure S2: EDX analysis of MOF1, MOF1/Ni, MOF1/Pd and MOF1/Pt; Figure S3: Elemental mapping of MOF1/Ni, MOF1/Pd and MOF1/Pt; Figure S4: Example of ^{1}H NMR spectrum after hydrogenation of CO_2 using THF and KOH base and pre-catalyst MOF1@Pd at 160 °C for 24 h recorded in D_2O at 25 °C in the presence of CH_3CN internal standard; Figure S5: Example of $^1H\{^{13}C\}$ NMR spectrum after hydrogenation of CO_2 using THF and KOH with pre-catalyst MOF1@Pd at 160 °C for 24 h recorded in D_2O at 25 °C.

Author Contributions: Conceptualization, G.M. and B.C.E.M.; methodology, N.M.; software, G.M.; validation, J.D. and B.C.E.M.; formal analysis, N.M.; investigation, N.M.; resources, B.C.E.M.; data curation, B.C.E.M.; writing original draft preparation, N.M.; writing—review and editing, G.M. and B.C.E.M.; supervision, G.M., J.D. and B.C.E.M.; funding acquisition, G.M. and B.C.E.M. All authors have read and agreed to the published version of the manuscript.

Funding: This research was funded by South Africa's National Research Fund (NRF) in partnership with The World Academy of Sciences (TWAS) provided financial support (Grant Numbers: 99978), grant Green Chemistry for Life Program (PhosAgro/UNESCO/IUPAC) grant number 4500378253, and the Future Leaders African Independent Research (FLAIR) program (FLR/R1/191510).

Conflicts of Interest: The authors declare no conflict of interest.

References

1. MacDowell, N.; Florin, N.; Buchard, A.; Hallett, J.; Galindo, A.; Jackson, G.; Adjiman, C.S.; Williams, C.K.; Shah, N.; Fennell, P. An overview of CO_2 capture technologies. *Energy Environ. Sci.* **2010**, *3*, 1645. [CrossRef]
2. Li, Y.-N.; Ma, R.; He, L.-N.; Diao, Z.-F. Homogeneous hydrogenation of carbon dioxide to methanol. *Catal. Sci. Technol.* **2014**, *4*, 1498. [CrossRef]
3. Muller, K.; Sun, Y.; Thiel, W.R. Ruthenium(II)-Phosphite Complexes as Catalysts for the Hydrogenation of Carbon Dioxide. *ChemCatChem* **2013**, *5*, 1340–1343. [CrossRef]
4. Federsel, C.; Jackstell, R.; Beller, M. State-of-the-art catalysts for hydrogenation of carbon dioxide. *Angew. Chem. Int. Ed.* **2010**, *49*, 6254–6257. [CrossRef] [PubMed]
5. Dhakshinamoorthy, A.; Opanasenko, M.; Cejka, J.; Garcia, H. Metal organic frameworks as heterogeneous catalysts for the production of fine chemicals. *Catal. Sci. Technol.* **2013**, *3*, 2509–2540. [CrossRef]
6. Barsukova, M.; Goncharova, T.; Samsonenko, D.; Dybtsev, D.; Potapov, A. Synthesis, Crystal Structure, and Luminescent Properties of New Zinc(II) and Cadmium(II) Metal-Organic Frameworks Based on Flexible Bis(imidazol-1-yl)alkane Ligands. *Crystals* **2016**, *6*, 132. [CrossRef]
7. Agarwal, R. Methanol Synthesis from CO_2 Hydrogenation Using Metal–Organic Frameworks. In *CO_2 Separation, Purification and Conversion to Chemicals and Fuels*; Springer: Singapore, 2019; pp. 79–92. ISBN 978-981-13-3295-1.
8. Rungtaweevoranit, B.; Baek, J.R.; Araujo, J.; S. Archanjo, B.; Min Choi, K.; M. Yaghi, O.; A. Somorjai, G. Copper Nanocrystals Encapsulated in Zr-based Metal–Organic Frameworks for Highly Selective CO2 Hydrogenation to Methanol. *Nano Lett.* **2016**, *16*, 7645–7649. [CrossRef]
9. Stock, N.; Biswas, S. Synthesis of Metal-Organic Frameworks (MOFs): Routes to Various MOF Topologies, Morphologies, and Composites. *Chem. Rev.* **2012**, *112*, 933–969. [CrossRef]
10. Pachfule, P.; Das, R.; Poddar, P.; Banerjee, R. Solvothermal Synthesis, Structure, and Properties of Metal Organic Framework Isomers Derived from a Partially Fluorinated Link. *Cryst. Growth Des.* **2011**, *11*, 1215–1222. [CrossRef]
11. Ni, Z.; Masel, R.I. Rapid Production of Metal−Organic Frameworks via Microwave-Assisted Solvothermal Synthesis. *J. Am. Chem. Soc.* **2006**, *128*, 12394–12395. [CrossRef]
12. Zhang, Z.; Zhang, S.; Yao, Q.; Chen, X.; Lu, Z.-H. Controlled Synthesis of MOF-Encapsulated NiPt Nanoparticles toward Efficient and Complete Hydrogen Evolution from Hydrazine Borane and Hydrazine. *Inorg. Chem.* **2017**, *56*, 11938–11945. [CrossRef] [PubMed]
13. Li, X.; Zhang, Z.; Xiao, W.; Deng, S.; Chen, C.; Zhang, N. Mechanochemistry-assisted encapsulation of metal nanoparticles in MOF matrices via a sacrificial strategy. *J. Mater. Chem. A* **2019**, *7*, 14504–14509. [CrossRef]
14. Dou, S.; Li, X.; Tao, L.; Huo, J.; Wang, S. Cobalt nanoparticle-embedded carbon nanotube/porous carbon hybrid derived from MOF-encapsulated Co_3O_4 for oxygen electrocatalysis. *Chem. Commun.* **2016**, *52*, 9727–9730. [CrossRef] [PubMed]
15. Chen, L.; Chen, H.; Luque, R.; Li, Y. Metal−organic framework encapsulated Pd nanoparticles: Towards advanced heterogeneous catalysts. *Chem. Sci.* **2014**, *5*, 3708–3714. [CrossRef]
16. Gutterød, E.S.; Lazzarini, A.; Fjermestad, T.; Kaur, G.; Manzoli, M.; Bordiga, S.; Svelle, S.; Lillerud, K.P.; Skúlason, E.; Øien-ØDegaard, S.; et al. Hydrogenation of CO_2 to Methanol by Pt Nanoparticles Encapsulated in UiO-67: Deciphering the Role of the Metal-Organic Framework. *J. Am. Chem. Soc.* **2020**, *142*, 999–1009. [CrossRef]
17. Olsbye, U.; Nova, A.; Gutterød, E.S.; Pulumati, S.H.; Kaur, G.; Lazzarini, A.; Solemsli, B.G.; Gunnæs, A.E.; Ahoba-Sam, C.; Kalyva, M.E.; et al. Influence of defects and H_2O on the hydrogenation of CO_2 to methanol over pt nanoparticles in UiO-67 metal-organic framework. *J. Am. Chem. Soc.* **2020**, *142*, 17105–17118. [CrossRef]
18. Tshuma, P.; Makhubela, B.; Mehlana, G.; Bingwa, N. Palladium(II) Immobilized on Metal–Organic Frameworks for Catalytic Conversion of Carbon Dioxide to Formate. *Inorg. Chem.* **2020**, *59*, 6717–6728. [CrossRef]
19. Tshuma, P.; Makhubela, B.C.E.; Öhrström, L.; Bourne, S.A.; Chatterjee, N.; Beas, I.N.; Darkwa, J.; Mehlana, G. Cyclometalation of lanthanum(III) based MOF for catalytic hydrogenation of carbon dioxide to formate. *RSC Adv.* **2020**, *10*, 3593–3605. [CrossRef]
20. Burrows, A.D.; Cassar, K.; Düren, T.; Friend, R.M.W.; Mahon, M.F.; Rigby, S.P.; Savarese, T.L. Syntheses, structures and properties of cadmium benzenedicarboxylate metal-organic frameworks. *Dalton Trans.* **2008**, *18*, 2465–2474. [CrossRef]

21. Mondloch, J.; Karagiaridi, O.; Farha, O.; Hupp, J. Activation of metal–organic framework materials. *CrystEngComm* **2013**, *15*, 9258–9264. [CrossRef]
22. Servalli, M.; Bokhoven, J.A. Van Fast and high yield post-synthetic modification of metal—organic frameworks by vapor diffusion w. *Chem. Commun.* **2012**, *48*, 1904–1906. [CrossRef] [PubMed]
23. Yu, J.; Mu, C.; Yan, B.; Qin, X.; Shen, C.; Xue, H.; Pang, H. Nanoparticle / MOF composites: Preparations and applications. *Mater. Horizons* **2017**, *4*, 557–569. [CrossRef]
24. Lei, Y.; Zhao, H.; Rivas, R.D.; Lee, S.; Liu, B.; Lu, J.; Stach, E.; Winans, R.E.; Chapman, K.W.; Greeley, J.P.; et al. Adsorbate-induced structural changes in 1–3 nm platinum nanoparticles Adsorbate-Induced Structural Changes in 1–3 nm Platinum. *J. Am. Chem. Soc.* **2014**, *136*, 9320–9326. [CrossRef] [PubMed]
25. Hou, Y.; Kondoh, H.; Ohta, T.; Gao, S. Size-controlled synthesis of nickel nanoparticles. *Appl. Surf. Sci.* **2005**, *241*, 218–222. [CrossRef]
26. Ezugwu, C.I.; Alam, N.; Yusubov, M.; Verpoort, F. Metal—organic frameworks containing N-heterocyclic carbenes and their precursors. *Coord. Chem. Rev.* **2016**, *307*, 188–210. [CrossRef]
27. Zhan, G.; Zeng, H.C. Alternative synthetic approaches for metal—organic frameworks: Transformation from solid. *Chem. Commun.* **2016**, *53*, 72–81. [CrossRef]
28. Zhao, Z.-W.; Zhou, X.; Liu, Y.-N.; Shen, C.-C.; Yuan, C.-Z.; Jiang, Y.-F.; Zhao, S.-J.; Ma, L.-B.; Cheang, T.-Y.; Xu, A.-W. Ultrasmall Ni nanoparticles embedded in Zr-based MOFs provide high selectivity for CO_2 hydrogenation to methane at low temperatures. *Catal. Sci. Technol.* **2018**, *8*, 3160–3165. [CrossRef]